Near IR Heptamethine Cyanine Dye–Mediated Cancer Imaging

Xiaojian Yang[1,4], Chunmeng Shi[1,5], Rong Tong[6], Weiping Qian[1], Haiyen E. Zhau[1,4], Ruoxiang Wang[1], Guodong Zhu[1], Jianjun Cheng[6], Vincent W. Yang[2], Tianmin Cheng[5], Maged Henary[3], Lucjan Strekowski[3], and Leland W.K. Chung[1,4]

Abstract

Purpose: Near-IR fluorescence imaging has great potential for noninvasive *in vivo* imaging of tumors. In this study, we show the preferential uptake and retention of two hepatamethine cyanine dyes, IR-783 and MHI-148, in tumor cells and tissues.

Experimental Design: IR-783 and MHI-148 were investigated for their ability to accumulate in human cancer cells, tumor xenografts, and spontaneous mouse tumors in transgenic animals. Time- and concentration-dependent dye uptake and retention in normal and cancer cells and tissues were compared, and subcellular localization of the dyes and mechanisms of the dye uptake and retention in tumor cells were evaluated using organelle-specific tracking dyes and bromosulfophthalein, a competitive inhibitor of organic anion transporting peptides. These dyes were used to detect human cancer metastases in a mouse model and differentiate cancer cells from normal cells in blood.

Results: These near-IR hepatamethine cyanine dyes were retained in cancer cells but not normal cells, in tumor xenografts, and in spontaneous tumors in transgenic mice. They can be used to detect cancer metastasis and cancer cells in blood with a high degree of sensitivity. The dyes were found to concentrate in the mitochondria and lysosomes of cancer cells, probably through organic anion transporting peptides, because the dye uptake and retention in cancer cells can be blocked completely by bromosulfophthalein. These dyes, when injected to mice, did not cause systemic toxicity.

Conclusions: These two heptamethine cyanine dyes are promising imaging agents for human cancers and can be further exploited to improve cancer detection, prognosis, and treatment. *Clin Cancer Res; 16(10); 2833–44. ©2010 AACR.*

Near-IR (NIR) excitable fluorescent contrast agents offer unique possibilities for *in vivo* cancer imaging. These agents show little autofluorescence in aqueous solution, and upon binding to macromolecules in cells, NIR dyes display drastically increased fluorescence due to rigidization of the fluorophores (1). The most common NIR fluorophores are polymethine cyanine dyes. In clinical practice, pentamethine and heptamethine cyanines composed of benzoxazole, indole, and quinoline are of great value and interest (2, 3). These organic dyes are characterized by high extinction coefficients and relatively large Stokes' shifts. With emission profiles at 700 to 1,000 nm, their fluorescence can be readily detected from deep tissues by commercially available imaging modalities (4–6).

Application of organic dyes in cancer detection and diagnosis has yet to be fully explored (5). The conventional approach to tumor imaging is through designed delivery of NIR fluorophores, mostly by chemical conjugation to tumor-specific ligands, including metabolic substrates, aptamers, growth factors, and antibodies (7–10). A number of surface molecules have been tested as targets,

Authors' Affiliations: [1]Molecular Urology and Therapeutics, Department of Urology, Winship Cancer Institute and [2]Division of Digestive Diseases, Department of Medicine, Emory University School of Medicine; [3]Department of Chemistry, Georgia State University, Atlanta, Georgia; [4]Uro-Oncology Research Program, Department of Medicine, Samuel Oschin Comprehensive Cancer Institute, Cedars-Sinai Medical Center, Los Angeles, California; [5]Chongqing Engineering and Technology Center for Nanomedicine, Third Military Medical University, Chongqing, China; and [6]Department of Material Science and Engineering, University of Illinois at Urbana-Champaign, Urbana, Illinois

Translational Relevance

Cancer mortality can be reduced by the development of noninvasive and effective imaging technologies that can detect tumors at metastatic sites and cancer cells in biological fluids. We report our discovery of two heptamethine cyanine dyes with near-IR fluorescence emission profiles that can detect the presence of human tumors grown in mice, spontaneous prostate and intestinal tumors in transgenic animals, and tumor cells in human blood, without the necessity of chemical conjugation. These unique heptamethine cyanine dyes can be further exploited for the detection of tumor cells in histopathologic specimens, circulating tumor cells in blood, and differentiating surgical margins in clinical specimens for improved diagnosis, prognosis, and treatment of cancer patients.

including membrane receptors, extracellular matrices, cancer cell–specific markers, and neovascular endothelial cell–specific markers (11–13). One limitation of these approaches is that the NIR moieties only detect specific cancer cell types with well-characterized surface properties, whereas tumors are notorious for their heterogeneity (14, 15). In addition, chemical conjugation may alter the specificity and affinity of the targeting ligands (3). A simpler and more straightforward strategy is needed to broaden the use of NIR dyes for noninvasive tumor imaging.

We identified a class of NIR fluorescence heptamethine cyanines as dual imaging and targeting agents and present our results with IR-783 and MHI-148, two prototypic heptamethine cyanine dyes. These organic dyes are spontaneously taken up and accumulated in cancer but not normal cells, providing the advantage of tumor-specific targeting that does not require chemical conjugation of the imaging dyes. Administration of the organic dyes to tumor-bearing mice, combined with noninvasive NIR imaging, enabled us to detect a panel of human and mouse tumors in various experimental settings. Exposure of human cancer cells to these dyes allowed us to differentiate normal from cancer cells and detect cancer cells in human blood with a high degree of sensitivity. These dyes were found to be nontoxic when given to mice. The dual imaging and targeting property of these organic dyes could be further exploited as improved modalities of cancer detection, diagnosis, and therapy. These two heptamethine cyanine dyes have almost identical imaging and targeting properties. In this report, we used IR-783 to show their many exploitable features.

Materials and Methods

Chemicals

The heptamethine cyanine dye IR 783 (2-[2-[2-chloro-3-[2-[1,3-dihydro-3,3-dimethyl-1-(4-sulfobutyl)-2H-indol-2-ylidene]-ethylidene]-1-cyclohexen-1-yl]-ethenyl]-3,3-dimethyl-1-(4-sulfobutyl)-3H-indolium) was purchased from Sigma-Aldrich and purified by the published methods. The heptamethine cyanine dye MHI-148 (2-[2-[2-chloro-3-[2-[1,3-dihydro-3,3-dimethyl-1-(5-carboxypentyl)-2H-indol-2-ylidene]-ethylidene]-1-cyclohexen-1-yl]-ethenyl]-3,3-dimethyl-1-(5-carboxypentyl)-3H-indolium bromide) was synthesized and purified as described previously (16–18). The other heptamethine cyanine dyes and their derivatives (see Supplementary Table S1) were also prepared by published procedures. All materials were dissolved in DMSO diluted with appropriate vehicles, filtered through 0.2-μm filters, and stored at 4°C before use.

Cell lines and cell culture

Human cancer cells used in this study were prostate cancer (LNCaP, C4-2, C4-2B, ARCaP$_E$, ARCaP$_M$, and PC-3), lung cancer (H358), breast cancer (MCF-7), cervical cancer (HeLa), leukemia (K562), renal cancer (SN12C, ACHN), bladder cancer (T24), and pancreatic cancer (MIA PaCa-2). As controls, normal human bone marrow stroma cells (HS-27A), normal human prostate epithelial cells (P69 and NPE), normal human prostate fibroblasts (NPF), human vascular endothelial cells (HUVEC-CS), and human embryonic kidney cells (HEK293) were used. LNCaP, ARCaP, and their lineage-derived cells (C4-2 and C4-2 B) were established by our laboratory and cultured in T-medium as described (19, 20). Human prostate epithelial cells, NPE, and human prostate fibroblasts (NPF) were derived from the normal areas of prostatectomy specimens by our laboratory using an Emory University–approved protocol and were maintained in T-medium as described (21). SN12C was obtained from a patient with renal clear cell carcinoma (22) and was cultured in T-medium. Unless otherwise specified, all of the other human cell lines were purchased from American Type Culture Collection and were cultured in American Type Culture Collection–recommended media, with 5% fetal bovine serum and 1× penicillin/streptomycin at 37°C with 5% CO$_2$. In this study, we also investigated the dye uptake by mouse pancreatic cancer cell lines PDAC2.3, PDAC3.3, BTC3, and BTC4 derived from transgenic mice, kindly provided to us by Dr. Douglas Hanahan from University of California at San Francisco. These cells were also cultured in T-medium.

Cell and tissue uptake study using NIR heptamethine cyanine dyes

Cells (1 × 10^4 per well) were seeded on vitronectin-coated four-well chamber slides (Nalgen Nunc) and incubated with T-medium containing 5% fetal bovine serum for 24 hours. After the cells had attached to the chamber slides, the cells were washed with PBS and exposed to the cyanine dye at a concentration of 20 μmol/L in T-medium. The slides were incubated at 37°C for 30 minutes and washed twice with PBS to remove excess dyes, and cells were fixed with 10% formaldehyde

at 4°C. The slides were then washed twice with PBS and covered with glass coverslips with an aqueous mounting medium (Sigma-Aldrich). Images were recorded by confocal laser microscopy (Zeiss LSM 510 META) using a 633-nm excitation laser and 670 to 810 nm long pass filter or a fluorescence microscope (Olympus 1× 71) equipped with a 75-W Xenon lamp and an indocyanine green filter cube (excitation, 750-800 nm; emission, 820-860 nm; Chroma).

To determine dye uptake in tissues, tissues isolated from tumor-bearing mice (see below) were placed in OTC medium and frozen at −80°C. Frozen 5-μm tissue sections were prepared for histopathologic observation using the microscope as described above.

Assessment of cyanine dye uptake into the mitochondria and lysosomes of cancer cells

Cells were plated on live-cell imaging chambers (World Precision Instrument) overnight. Cells were exposed to cyanine dyes at different concentrations, and dye uptake was evaluated by a Perkin-Elmer Ultraview ERS spinning disc confocal microscope. This system was mounted on a Zeiss Axiovert 200 m inverted microscope equipped with a 37°C stage warmer, incubator, and constant CO_2 perfusion. A 63× or 100× Zeiss oil objective (numerical aperture, 1.4) was used for live cell images, and a Z-stack was created using the attached piezoelectric z-stepper motor. The 633-nm laser line of an argon ion laser (set at 60% power) was used to excite the cyanine dyes. Light emission at 650 nm, although not optimal for these dyes, was detected and was found to correlate directly with the dye concentrations in the cells (Supplementary Fig. S1). For comparative studies, the exposure time and laser intensity were kept identical for accurate intensity measurements. Pixel intensity was quantified using Metamorph 6.1 (Universal Imaging), and the mean pixel intensity was generated as gray level using the Region Statistics feature on the software (23). To determine the dye uptake by the mitochondria, the mitochondrial tracking dye Mito Tracker Orange CMTMROS (Molecular Probes) was used. To determine the dye localization in lysosomes, a lysosome-tracking dye, Lyso Tracker Green DND-26 (Molecular Probes), was selected. Imaging of mitochondrial and/or lysosome localization of the cyanine dye was conducted under confocal microscopy (24).

To determine if the cyanine dye uptake and accumulation in cancer cells were dependent upon organic anion transporting peptides (OATP), we preincubated cells with 250 μmol/L bromosulfophthalein (BSP), a competitive inhibitor of OATPs (25), for 5 minutes before incubating the cells with cyanine dyes. The uptake and accumulation of cyanine dyes in the presence and absence of BSP were conducted in the stage warmer incubator for a period of 35 minutes. The levels of cyanine dye taken up and accumulated in normal prostate (P69) and prostate cancer (ARCaP$_M$) cells were determined and compared on a real-time basis.

Uptake and accumulation of cyanine dyes in tumors in live mice

Human cancer cells were implanted (1×10^6) either s.c., orthotopically, or intraosseously into 4- to 6-week-old athymic nude mice (National Cancer Institute) according to our previously published procedures (26, 27). All animal studies were conducted under the Emory University Animal Care and Use Committee guidelines. When tumor sizes reached between 1 and 6 mm in diameter, as assessed by X-ray or by palpation, mice were injected i.v. or i.p. with cyanine dyes at a dose of 0.375 mg/kg or 10 nmol/20 g mouse body weight. Whole body optical imaging was taken at 24 hours using a Kodak Imaging Station 4000 MM equipped with fluorescent filter sets (excitation/emission, 800:850 nm). The field of view was 120 mm in diameter. The frequency rate for NIR excitation light was 2 mW/cm^2. The camera settings included maximal gain, 2×2 binning, $1,024 \times 1,024$ pixel resolution, and an exposure time of 5 seconds. In some instances, live mice were also imaged by an Olympus OV100 Whole Mouse Imaging System (excitation, 762 nm; emission, 800 nm; Olympus Corp.), containing a MT-20 light source (Olympus Biosystems) and DP70 CCD camera (Olympus). Before imaging, mice were anesthetized with ketamine (75 mg/kg). During imaging, mice were maintained in an anesthetized state.

We also studied the spontaneous metastasis of ARCaP$_M$ tumor cells stably transduced with an AsRed2 red fluorescence protein (RFP; Clontech) by injecting these cells orthotopically in mice. ARCaP$_M$-RFP metastasis was determined by the same procedures described above for capturing cyanine dye tumor imaging after IR-783 i.p. injection at a dose of 10 nmol/20 g. In addition, at the time of sacrifice, both frozen and paraffin-embedded tissue sections were obtained for RFP and confocal fluorescence imaging. Positive identification of ARCaP$_M$-RFP cells was accomplished by fluorescence microscopy and validated by subculturing ARCaP$_M$-RFP cells directly from bone metastasis tissue specimens.

The uptake of cyanine dyes by the TRAMP mouse prostate model and the Apc$^{Min/+}$ mouse adenoma model (obtained from The Jackson Laboratory) was assessed by a similar protocol as described above. We also used the Olympus OV100 imaging system to detect adenoma in the Apc$^{Min/+}$ mouse model. In brief, mice were injected i.p. with IR-783 dye at a dose of 10 nmol/20 g body weight, and animals were subjected to total body cyanine dye imaging as described above. Animals were sacrificed at 48 hours after dye administration, and tumors were dissected and subjected to NIR imaging. The presence of tumor cells in tissue specimens was confirmed by histopathologic analysis.

Assessments of heptamethine cyanine dye biodistribution in normal and tumor-bearing mice *in vivo*

To assess tissue distribution of these dyes, athymic mice without tumor implantation were sacrificed at 0, 6, and 80 hours ($n = 3$ each) after i.v. injection of IR-783 dye at a dose of 10 nmol/20 g. Dissected organs were subjected to NIR

imaging by a Kodak Imaging Station 4000 MM. In another study, the mice bearing orthotopic ARCaP$_M$ tumors were subjected to NIR imaging at 0.5, 24, 48, 72, and 96 hours after IR-783 i.v. administration at a dose of 10 nmol/20 g. In some cases, we also assessed the biodistribution of NIR dye by a spectral method in tissues harvested from athymic mice bearing s.c. ARCaP$_M$ tumors (n = 6). Tumors and normal host organs were homogenized in PBS and centrifuged at 15,000 × g for 15 minutes to recover the supernatant fraction after the mice were injected i.p. with IR-783 at a dose of 10 nmol/20 g. The presence of the organic dyes (parental IR-783 and its metabolites) in tissues was estimated spectrophotometrically at an emission wavelength of 820 nm by a PTI Near-IR Fluorometer QuantaMaster 50 (PTI) equipped with a 75-W xenon arc lamp under 500 to 1,700 nm InGaAs detector using known concentrations of IR-783 as the standard (28). In other cases, tumor tissues harvested from mice were stored in formalin from 1 week to 3 months, and fluorescence images were obtained and compared.

Detection of cancer cells in human blood

An experimental model of evaluating human prostate cancer cells in blood was developed. In brief, heparinized whole blood from human volunteers was collected according to an Emory University–approved institutional review board protocol. A known number of human prostate cancer cells (10-1,000) were added to 1 mL of whole blood, mixed gently with 20 μmol/L IR-783, and incubated for 30 minutes at 37°C. The mononuclear cells and cancer cells were recovered by gradient centrifugation using Histopaque-1077 (Sigma). The isolated live cells were observed under a confocal fluorescence microscope.

Assessment of systemic toxicity of IR-783 in mice

We investigated the systemic toxicity of IR-783 in C57BL/6 mice (National Cancer Institute) by injecting the dye by an i.p. route. The mice (n = 8 per group) were subdivided into four groups and received PBS as control and IR-783 i.p. injection daily at the following doses: 0.375 mg/kg (imaging dose), 3.75 mg/kg, and 37.5 mg/kg. They were weighed daily, and their physical activities were observed for 1 month following dye injection. The histomorphologic appearance of their vital organs was assessed at the time of sacrifice.

Data processing and statistics

The statistical significance of all data was determined by Student's t test. Data were expressed as the average ± SEM of the indicated number of determinations. The statistically significant difference was assigned as $P < 0.05$.

Results

Structural requirement of heptamethine cyanine dyes for tumor-specific uptake and retention

Using human cancer and normal human cell lines to study dye uptake and retention, we found that IR-783

and MHI-148 were unique in that they had both tumor imaging and targeting properties (Supplementary Table S1). A comparative analysis also uncovered several common structural features of heptamethine cyanine dyes accounting for their preferential uptake and retention by cancer cells. We classified the dyes operationally as active and inactive based upon their specific uptake and retention in cancer but not normal cells. A rigid cyclohexenyl ring in the heptamethine chain with a central chlorine atom maintains photostability, increases quantum yield, decreases photobleaching, and reduces dye aggregation in solution (1). Chemical substitution of the central chlorine atom with a thiobenzylamine group on the cyclohexenyl ring dramatically reduced the fluorescence intensity and eliminated their uptake by cancer cells and tumor xenografts, and so would a substitution of the side chain with hydroxyl, an ester, or an amino group rather than a charged carboxyl (i.e., MHI-148) or sulfonic acid (i.e., IR-783) moiety (see Supplementary Table S1 and Supplementary Figs. S2 and S3). In this report, we focus on characterizing the tumor-specific uptake and retention of two cyanine dyes, IR-783 (available commercially) and MHI-148 (available by chemical synthesis, see above).

Preferential uptake and retention of NIR fluorescence dyes by human cancer cells and tumor xenografts

Human cancer and normal cell studies. Cancer cell surface properties and surrounding leaky vasculatures have been exploited for the delivery of imaging agents (29–32). IR-783 and MHI-148 were tested for their ability to detect cancer cells (Fig. 1A). The two dyes were found not to accumulate in normal human bone marrow cells (HS-27A), vascular endothelial cells (HUVEC-CS), embryonic fetal kidney cells (HEK293), a primary culture of human prostate epithelial cells (NPE), or normal prostate fibroblasts (NPF; Fig. 1B). These dyes, however, were found to be retained in cancerous cells of human origin, including the prostate (C4-2, PC-3, and ARCaP$_M$), breast (MCF-7), lung (H358), cervical (HeLa), liver (HepG2), kidney (SN12C), pancreas (MIA PaCa-2), and leukemia (K562; Fig. 1C). These dyes were also found to be taken up by other malignant cells from both human and mouse, including human bladder cancer cell (T-24), renal cancer cell (ACHN), and mouse pancreatic cancer cell lines (PDAC2.3, PDAC3.3, BTC3, and BTC4 derived from transgenic mouse; Supplementary Fig. S4). There was no discernible difference in the amount and specificity of uptake of these two heptamethine cyanine NIR dyes by cancer cell lines. In this report, we focused predominately on the uptake and retention of IR-783 in cancer cells and tumor xenografts.

We next compared the kinetics of IR-783 uptake by cultured human prostate cancer ARCaP$_M$ versus P69 cells, a normal human prostate epithelial cell line (Fig. 2A). This study revealed a differential time-dependent uptake and retention of IR-783 by ARCaP$_M$ and P69 cells (Fig. 2B). Uptake and retention of IR-783 in ARCaP$_M$ cells occurred in two phases, an early phase completed in 12 minutes and

Fig. 1. Active uptake of hepatamethine cyanine dyes by human cancer cells but not normal cells in culture. A, the chemical structures of two hepatamethine cyanine dyes, IR-783 and MHI-148. B, normal human cells including bone marrow stromal cells (HS-27A), normal prostate epithelial cells (NPE), normal prostate stromal fibroblasts (NPF), vascular endothelial cells (HUVEC-CS), and human embryonic kidney cells (HEK293) showed very low uptake of these dyes in culture. C, human cancer cell lines including prostate (C4-2, PC-3, ARCaP$_M$), breast (MCF-7), cervical (HeLa), lung (H358), liver (HepG2), pancreatic (MIA PaCa-2), and renal (SN12C) cancer cells, as well as a human leukemia cell line (K562), showed significant uptake of IR-783 dye under similar staining and imaging conditions. Results are shown with images obtained from cells stained with 4′,6-diamidino-2-phenylindole (DAPI) of cell nuclei, the heptamethine cyanine IR-783 stain (NIR), and a merger of the two images (Merge). All the images were acquired at 630× magnification.
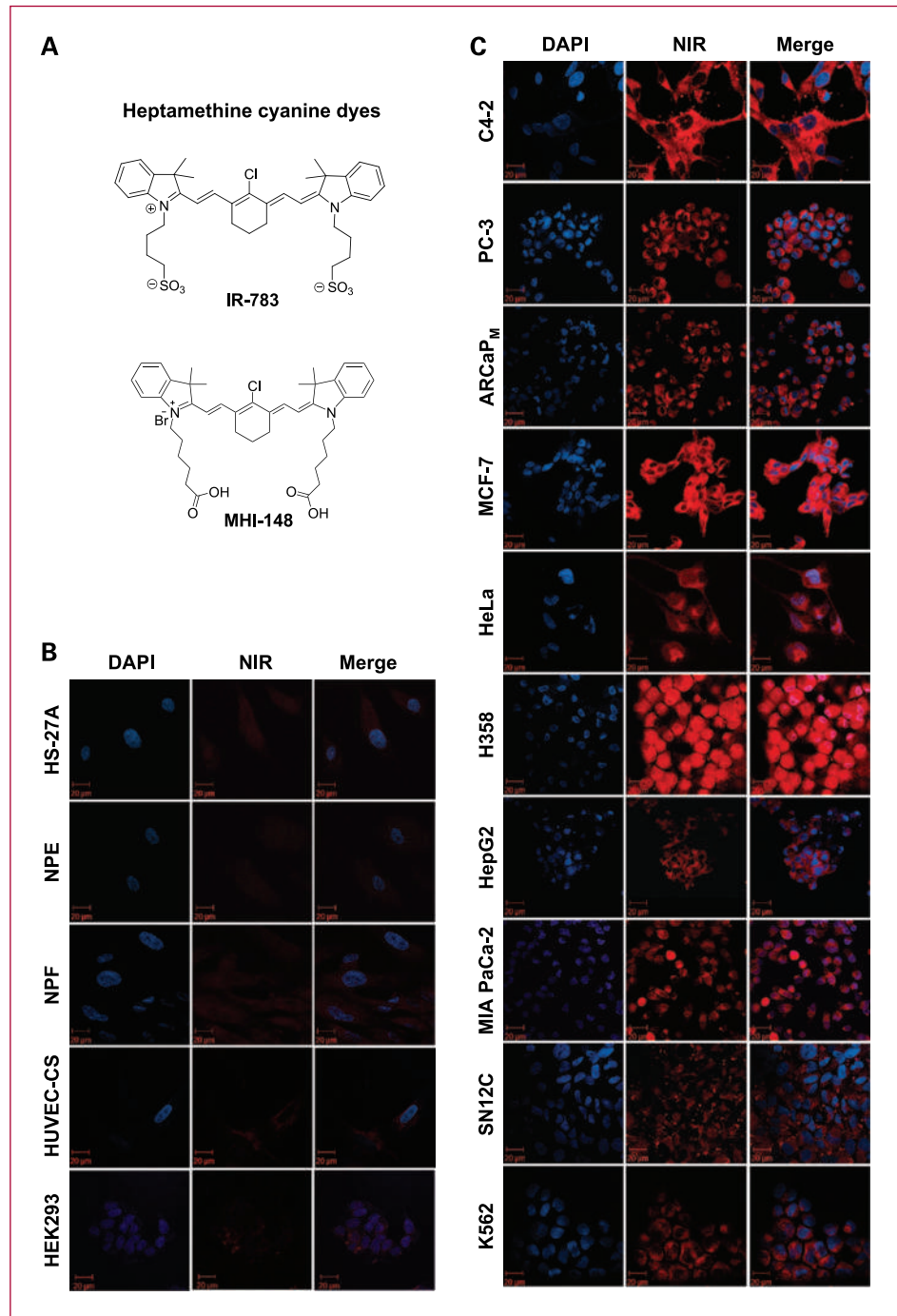
a late phase completed in 30 minutes. In the control P69 cells, the uptake and retention of IR-783 only began at 12 minutes, with a much lower plateau. Interestingly, the uptake and accumulation of IR-783 could be abolished by BSP, a competitive inhibitor of the OATPs (ref. 25; Fig. 2C). These results are consistent with the observation that IR-783 uptake into cancer cells was high at 37°C but none at 0°C (data not shown). These results confirmed that the cancer cell–specific uptake was an energy-dependent active process, most probably mediated by members of the OATP family.

We then evaluated the subcellular compartments where IR-783 was retained. Based on the dye colocalization using the tracking dyes, the NIR signal seemed to condense on mitochondrial and lysosomal organelles, with homogenous staining also detected throughout other cytoplasmic and nuclear compartments (Fig. 2D). These heptamethine cyanine NIR dyes apparently localized primarily within

mitochondrial and lysosomes but can bind to a host of other intracellular proteins.

Human tumor xenograft studies. IR-783 was injected i.p. or i.v. in athymic mice bearing human bladder tumors (T-24, s.c.), pancreas tumors (MIA PaCa-2, s.c.), prostate tumors (ARCaP$_M$, orthotopically), and kidney tumors (SN12C, intraosseouslly to tibia). The animals were imaged noninvasively with a NIR small animal imaging system (Fig. 3). Successive observations at different time points revealed that after the initial systemic distribution and clearance, intense signals were clearly associated with the tumors implanted at various anatomic sites, with no background interfering fluorescence from the mice. The presence of tumor cells in the tissue specimens was confirmed by histopathologic analysis with tissue sections stained with H&E.

Human cancer metastasis studies. To investigate if NIR dye could detect spontaneously metastasized tumors and to confirm if the NIR dye is associated with prostate

cancer bone metastasis, we inoculated mice orthotopically with ARCaP$_M$ cells that were stably tagged with AsRed2 RFP (Fig. 4A, a). On signs of cachexia at 3 months, the animals were subjected to noninvasive whole body NIR imaging with IR-783 (Fig. 4A, b). In addition to the presence of localized orthotopic tumors (see thick arrow), RFP-tagged ARCaP$_M$ tumors also appeared in mouse bone (see thin arrow). Upon *ex vivo* imaging, we detected both the primary tumor and the metastases in mouse tibia/femur. The presence of tumor cells in the mouse skeleton was confirmed by histopathologic evaluation and by the presence of RFP-tagged cells upon subculture of cells derived from the skeletal metastasis specimens (Fig. 4A, c and d).

Detection of spontaneous prostate and intestinal tumors in transgenic mouse models

To investigate if IR-783 could be used to detect spontaneously developed tumors, we adopted two transgenic
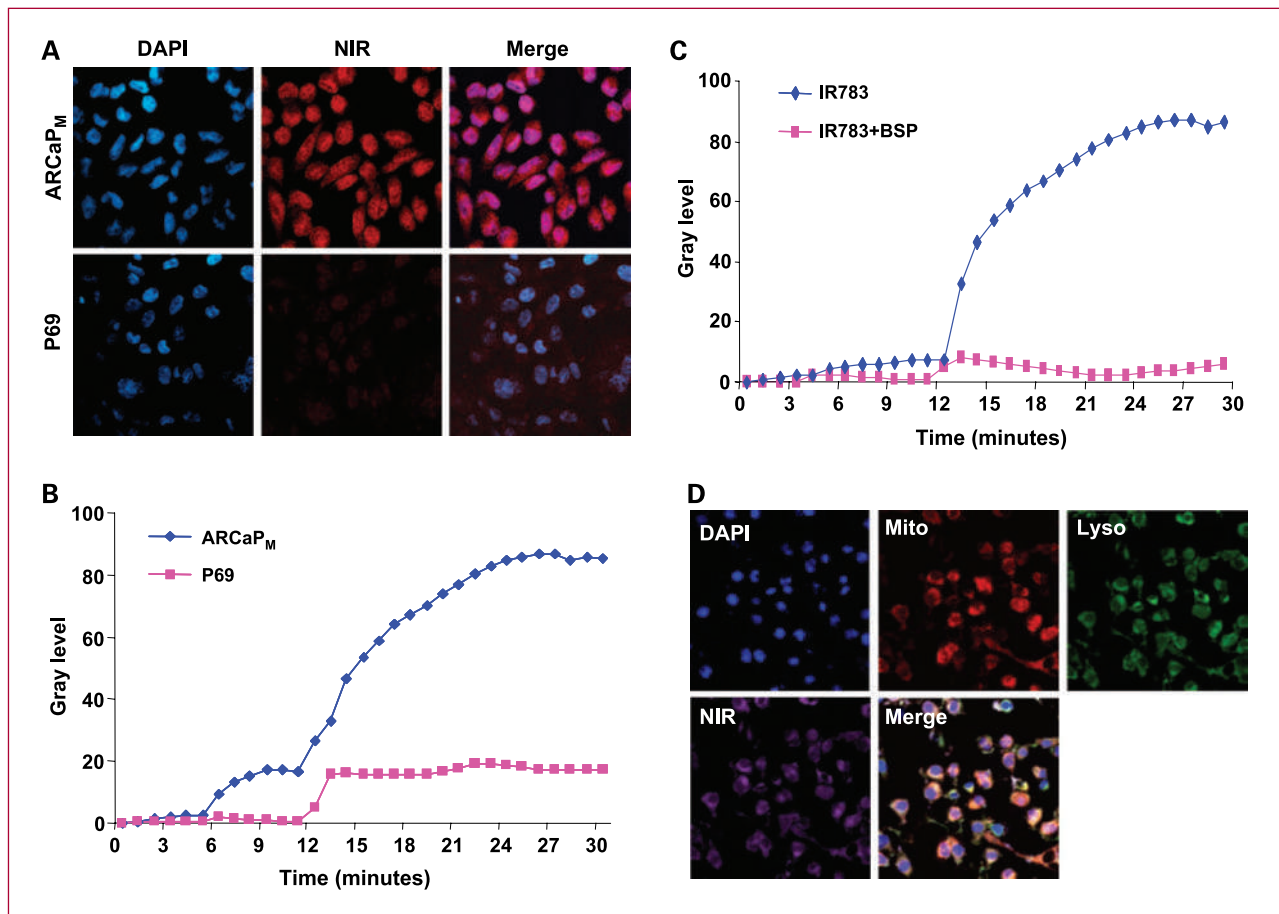
Fig. 2. Kinetics and subcellular localization of the NIR dyes. A, confocal imaging shows significant uptake of IR-783 dye in ARCaP$_M$ cells but not in normal human prostate epithelial P69 cells at 630× magnification. B, histogram shows differential and time-dependent uptake of IR-783 by human prostate cancer ARCaP$_M$ cells and P69 cells. C, uptake of the IR-783 dye (20 μmol/L) by ARCaP$_M$ cells can be abrogated by 250 μmol/L BSP. D, subcellular colocalization of the NIR hepatamethine cyanine dyes with lysosomes (Lyso) and mitochondrial (Mito) tracking dyes. ARCaP$_M$ cells that were stained with IR-783 were stained with a lysosome-specific dye, Lyso Tracking Green DND-26, and a mitochondria-specific dye, Mito Tracker Orange CMTMROS (630×). Fluorescence imaging indicates that a large portion of the IR-783 was colocalized with these subcellular organelles.
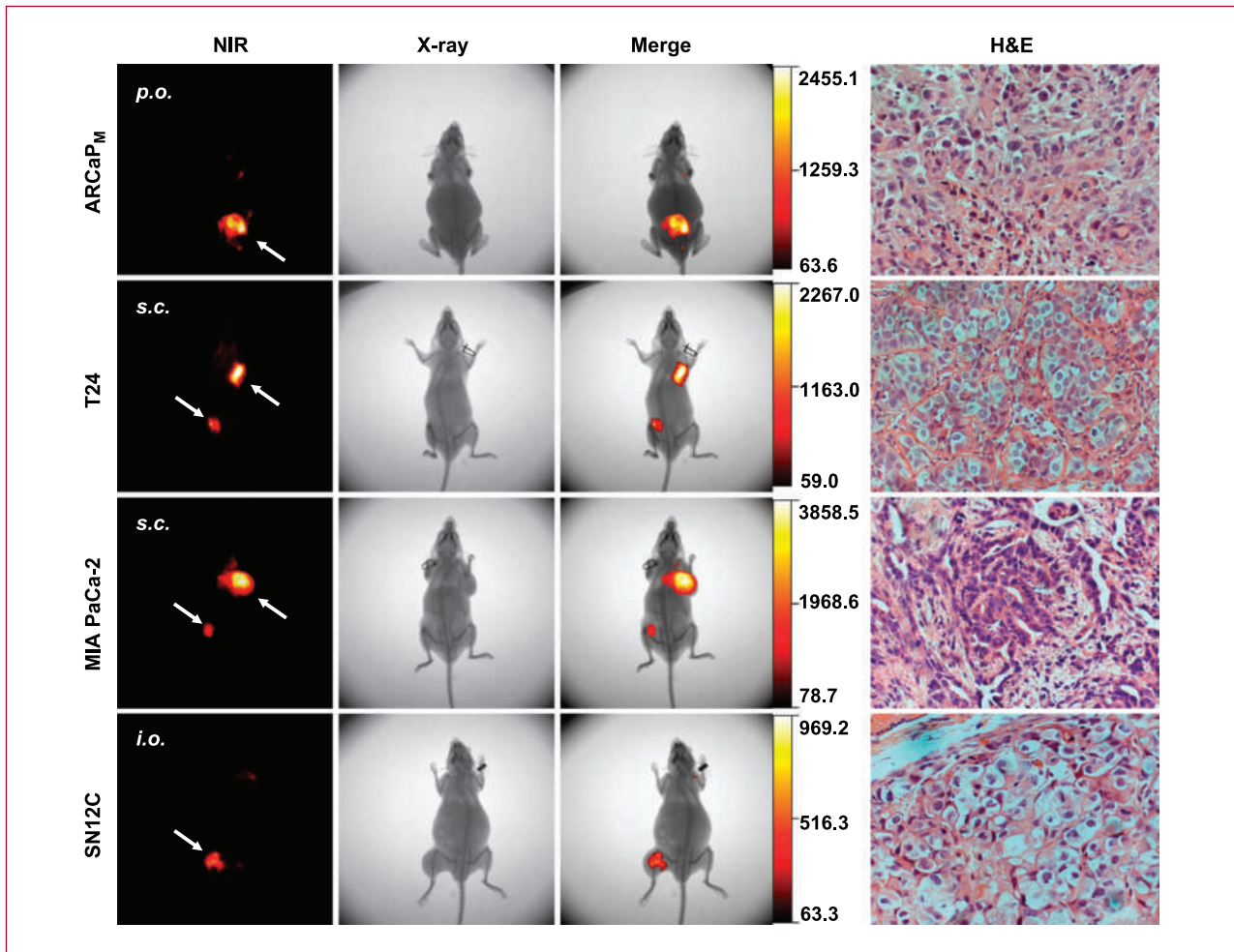
Fig. 3. Preferential uptake and retention of the hepatamethine cyanine dyes in human tumor xenografts. Mice bearing human prostate (ARCaP$_M$, orthotopic prostate tumor, p.o.), bladder (T24, s.c.), pancreatic (MIA PaCa-2, s.c.), and renal (SN12C, intraosseous to tibia, i.o) tumors were injected i.p. with IR-783 at a dose of 10 nmol/20 g. NIR imaging was done 24 hours later. Each mouse was subjected to fluorescence imaging (NIR) and X-ray imaging (X-ray) using the Kodak Imaging Station Imaging System, and the two images were superimposed (Merge) for tumor localization. After imaging, tissues with specific fluorescence signals were dissected, fixed in 10% formaldehyde, and subjected to histopathologic analysis by H&E staining (200×). In mice bearing s.c. tumors, we detected both tumors based on fluorescence imaging (see arrows).

mouse models that were known to display high degrees of tumor penetrance, the TRAMP mouse model for prostate cancer and the Apc$^{Min/+}$ mouse model for colon cancer (33, 34). Because the TRAMP and Apc$^{Min/+}$ mouse models represent the development of adenocarcinoma/neuroendocrine prostate tumors and adenoma of the intestine, respectively, this study also allowed us to assess if IR-783 could detect the early stage of tumor development (i.e., adenoma). IR-783 could detect tumor in both the TRAMP mice and the Apc$^{Min/+}$ mice (Fig. 4B and C). Specific detection of tumor but not normal cells was also confirmed by histopathologic analysis of the tumor specimens (Fig. 4B, f and C, c and d). An additional advantage of IR-783 imaging was its optical stability even after prolonged tissue fixation. TRAMP tumor specimens retain heptamethine cyanine

NIR fluorescence even after being stored in neutralized formalin solution for 3 weeks (Fig. 4B, e).

NIR dye tissue distribution studies

Hepatamethine cyanine dye tissue distribution studies were conducted in normal and tumor-bearing mice. Time-dependent dye clearance from normal mouse organs is shown in Fig. 5A. At 6 hours, NIR dye IR-783 was found to accumulate in mouse liver, kidney, lung, and heart. By 80 hours, dye was cleared from all mouse vital organs. The dye, however, was found to accumulate in tumor tissues at 24 hours with minimal background autofluorescence. Tumors retained IR-783 dye even at 4 days (or 96 hours; Fig. 5B). In both *in vivo* whole body and *ex vivo* analysis, we detected signal-to-noise ratios exceeding 25 in tumor specimens; however, normal organs, liver, lung, heart,
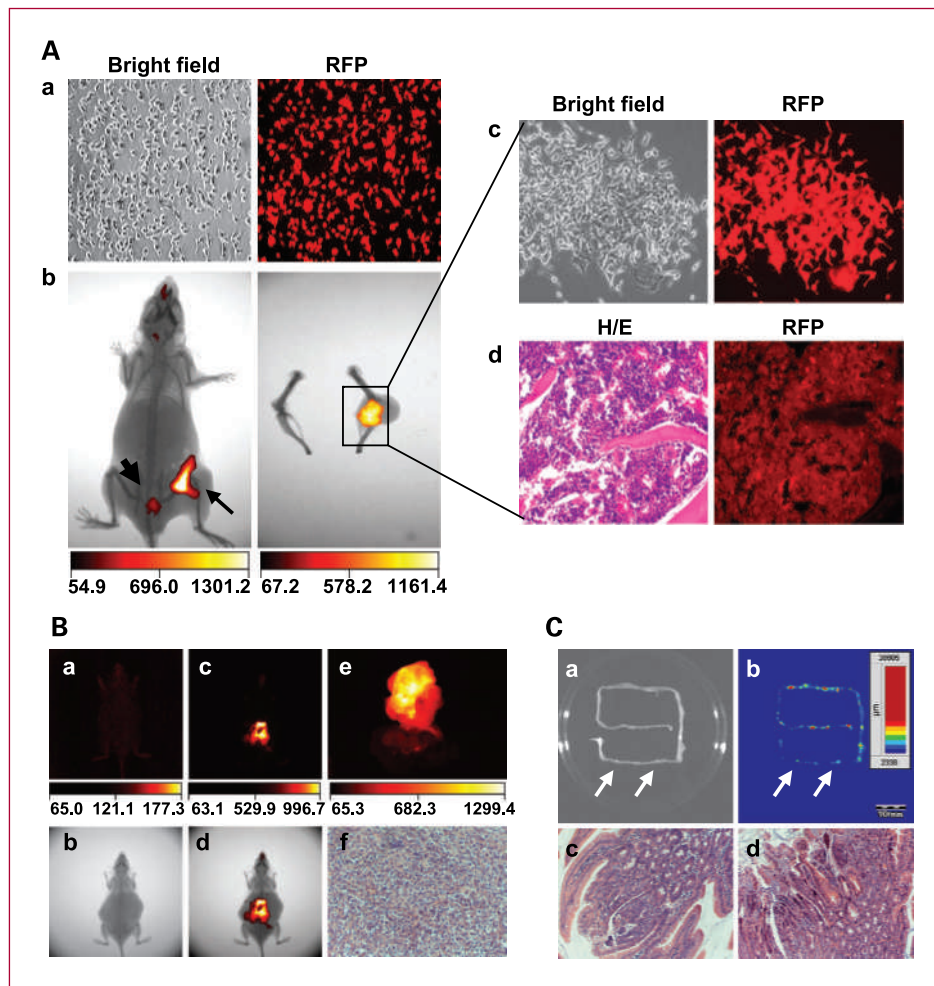
Fig. 4. Detection of tumor metastasis in mice and spontaneous tumors in transgenic animals. A, confirmation of the presence of bone metastatic prostate tumors in mice by NIR imaging after IR-783 i.p. injection at a dose of 10 nmol/20 g. a, the ARCaP$_M$ human prostate cancer cell line was stably transfected with AsRed2 RFP. The clone being used in this study exhibited typical ARCaP$_M$ cell morphology (bright field, 100×) and could emit intense red fluorescence. b, cells from this clone were inoculated orthotopically to athymic mice to produce both localized prostate tumor (thick arrow) and bone metastatic tumor (thin arrow), which were detected by IR-783 fluorescence imaging of the whole animal (left) and of the dissected skeletal bone (right). c, to confirm the detection of metastasis, marrow cells from the affected tibia/femur were cultured, and isolated cancer cells were found to express RFP. d, ARCaP$_M$ cells in the metastatic tibial/femur tumor could also be seen in formaldehyde fixed sections, either by conventional H&E stain or directly by red florescence imaging. These analyses unanimously confirmed that the signals attained in IR-783 imaging reflect metastases of the orthotopic ARCaP$_M$ tumor. B, detection of spontaneous prostate and intestine tumors in transgenic mouse models. a, whole body NIR fluorescent imaging of TRAMP mouse before dye injection, which revealed no background NIR fluorescence. b, whole body X-ray imaging of the animal. c, whole body NIR fluorescent imaging of TRAMP mouse revealed only tumor-positive signal after IR-783 i.p. injection at a dose of 10 nmol/20 g. d, fluorescence imaging picture of TRAMP mice merged with X-ray picture. e, the prostate tumor dissected from this TRAMP mouse showed a strong NIR signal even after fixation in 4% formalin solution for 3 weeks. f, the presence of tumor cells was confirmed by histopathology (H&E stain, 100×). C, detection of multiple intestinal neoplasia in Apc[Min/+] mice after the administration of IR-783 i.p. at a dose of 10 nmol/20 g with the Olympus OV110 imaging system. a, bright field photograph of a dissected intestine in the imaging chamber. b, NIR hepatamethine cyanine dye imaging of multiple tumors along the intestine, with two tumor nodules indicated with white arrows. c and d, these two nodules were excised, and adenoma was confirmed in these specimens by H&E staining (100×).

spleen, and kidneys displayed very low signals (Fig. 5C). In these studies, NIR dyes in tumor implants could be retained for as long as 15 days after dye administration (data not shown).

Before the quantification of the heptamethine cyanine dyes in excised tumors and normal organs, we established a standard curve by monitoring the emission profile of IR-783 at 820 nm (28, 35). Within concentration ranges from 0 to 40 μmol/L, a linear correlation ($r = 0.9991$) was found between the concentration of IR-783 and its emission intensity (Fig. 5D, left). Using this standard curve, we estimated spectrophotometically the apparent concentrations of the dye and its metabolites in tissues. Figure 5D (right) shows that the apparent concentrations of the NIR dye and its metabolites (defined here as light emission intensity at 820 nm) in tumors were significantly
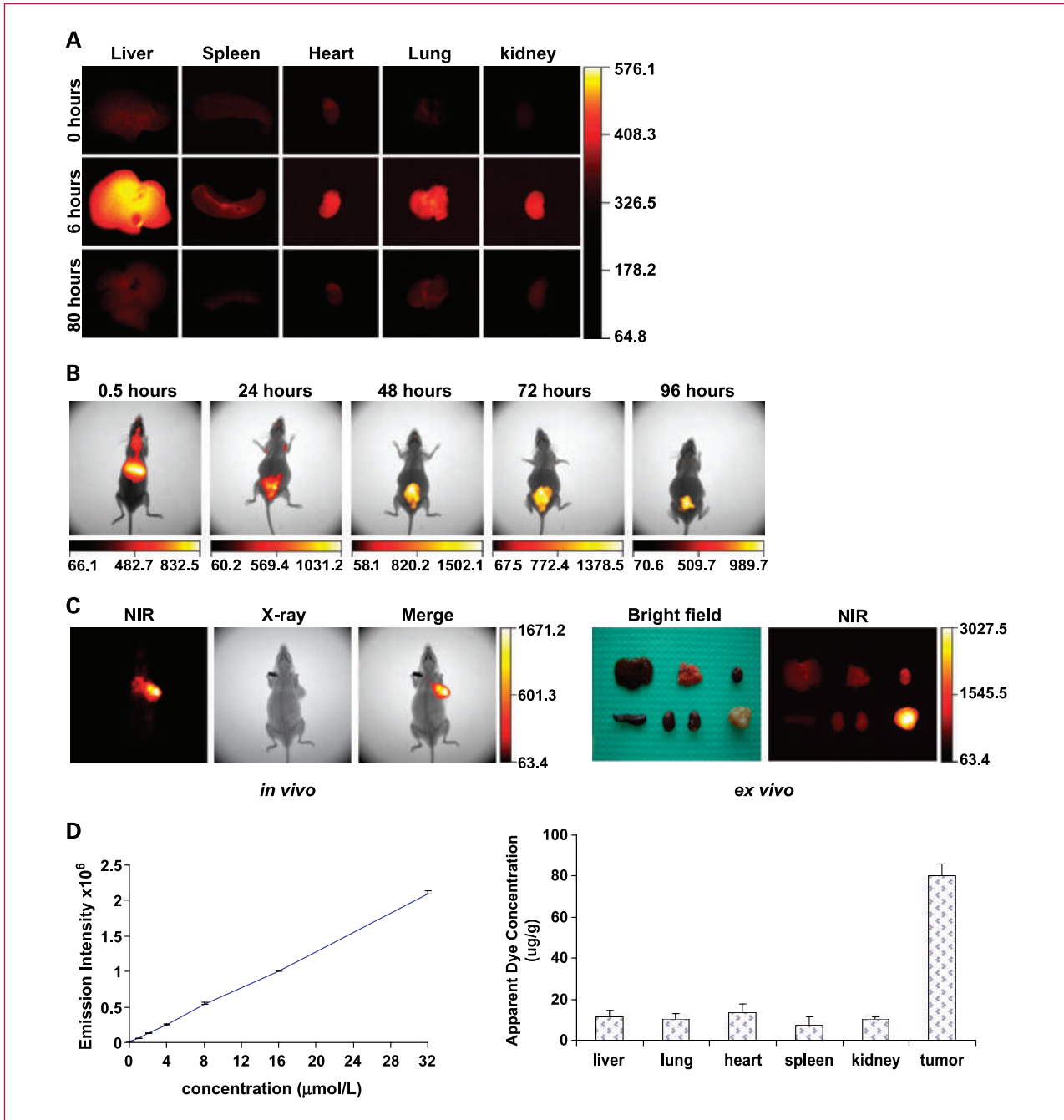
Fig. 5. Distribution of heptamethine cyanine dye IR-783 and its metabolites in tissues; time course and concentration-dependent studies in normal and tumor-bearing mice. A, normal organs dissected at 0, 6, and 80 hours after IR-783 i.v. injection at a dose of 10 nmol/20 g were subjected to NIR dye imaging with a Kodak Imaging Station 4000 MM (see Materials and Methods). Note that at 80 hours, IR-783 was completely cleared from all vital organs examined. B, a representative mouse bearing orthotopic ARCaP$_M$ human prostate tumor was imaged after IR-783 10 nmol/20 g i.v. injection at 0.5, 24, 48, 72, and 96 hours. Note dye uptake and retention seen in an ARCaP$_M$ orthotopic tumor. C, a representative mouse bearing a s.c. ARCaP$_M$ tumor subjected to NIR imaging after IR-783 i.p. injection at a dose of 10 nmol/20 g. The left panel shows the retention of IR-783 in the tumor 24 hours after dye administration in whole body *in vivo* imaging. The right panel shows the *ex vivo* imaging of surgically dissected tissues, which confirmed the uptake and retention of IR-783 in a surgically dissected ARCaP$_M$ tumor. Top row from left, liver, lung, and heart; bottom row from left, spleen, kidneys, and tumor. Tumor tissue displayed strong signals in both *in vivo* and *ex vivo* imaging. D, a standard curve was constructed based on the fluorescence emission intensity of IR-783 at 820 nm (see Materials and Methods) with the dye added to a PBS solution at concentrations of 0.5, 1, 2, 4, 8, 16, and 32 μmol/L. The correlation coefficient between the fluorescence emission intensity and concentration of IR-783 was estimated to be *r* = 0.9991 (left). The apparent dye concentration (μg/g) in organs and tumor was calculated based on the standard curve established above (right). The apparent dye concentration is defined here by the light emission intensity at 820 nm, which could include the parental IR-783 and its metabolites. Data are expressed as average ± SEM of three determinations.

higher than those in normal tissues with a difference approaching 10-fold ($P < 0.05$, data are expressed as average ± SEM of three determinations). This fluorescence emission could be contributed by the parental dye, its metabolites, and their binding to nucleic acids and proteins (36).

In dye systemic toxicity study, we observed no systemic toxicity of IR-783 dye in normal C-57BL/6 mice and this dye also did not affect body weights of the mice. No abnormal histopathology was seen in vital organs harvested from mice at the time of sacrifice.

Detection of cancer cells in human blood

Because IR-783 was confirmed to detect human cancer but not normal cells, we then tested whether this dye could be further exploited to detect circulating cancer cells in the blood using an experimental model. Figure 6A shows that cancer cells can be clearly visualized after mixture with human blood cells by IR-783 NIR imaging. We estimate that this dye is sufficiently sensitive to detect as few as 10 cancer cells per milliliter in whole blood (Fig. 6B).
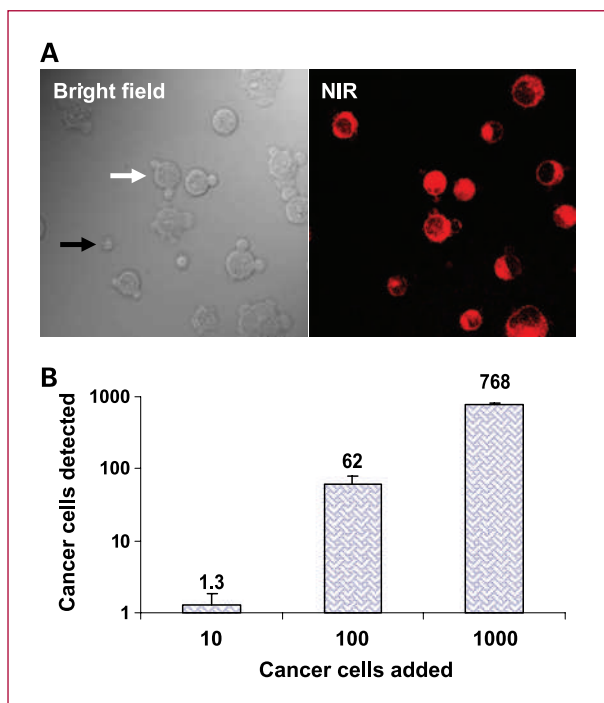
Fig. 6. Detection of human prostate cancer cells in human blood. A, ARCaP$_M$ cells mixed with human blood were incubated with IR-783, and the particulate fractions containing normal healthy mononuclear cells and cancer cells were isolated using gradient centrifugation. The cells were resuspended in PBS for acquisition of fluorescent images under a confocal microscope. Significant uptake and retention of the dye could be detected in ARCaP$_M$ cells in a fluorescent field (white arrow), whereas mononuclear cells hardly showed any signals (black arrow). B, to determine the sensitivity of this novel method for tumor cell detection, known numbers of ARCaP$_M$ cells (10-1,000 cells) were added to 1 mL of whole blood. Following gradient centrifugation, washing, and resuspension, positive fluorescent cancer cells were counted. Results presented in the histogram represent three separate experiments ($n = 3$) with data expressed as mean ± SEM.

Discussion

Chemically conjugated cyanine dyes have proved to be useful for measuring blood flow and cardiac output, as well as imaging tumors (2, 3, 37). The chemical structures of water-soluble pentamethine and heptamethine cyanine dyes have recently been modified to increase their chemical stability, photostability, and quantum yield (1). IR-783 and MHI-148 are two such new dyes, modified with a rigid cyclohexenyl substitution in the polymethine linker. The present study describes for the first time that these NIR dyes can be actively taken up and accumulated by cancer cells but not by normal cells. The salient features of these newly discovered dual imaging and targeting NIR dyes are as follows: (*a*) Detecting cancer cells and cancer metastases directly without the requirement of chemical conjugation. (*b*) Detecting many other tumor types and tumor cell populations under cell culture and *in vivo* conditions. The cancer-specific uptake and retention of these dyes is likely to be mediated by OATPs because the transport of these dyes into cancer cells can be antagonized by BSP, an OATP competitive inhibitor (38, 39). (*c*) Serving as potential carriers for drug payloads or radioactive agents to increase the specificity and reduce the toxicity of therapeutic agents by preferential uptake and accumulation in cancer cells but not in normal cells.

The cyanine dyes are water soluble, so they have rapid clearance and are unlikely to be trapped in the reticular endothelium of the liver, lung, or spleen. They were found to be superior for cancer detection to other cyanine dyes, such as indocyanine green, and noncyanine dyes, such as rhodamine 123 (data not shown). Imaging with NIR dyes can yield much higher signal/noise ratios with minimal interfering background fluorescence. The fluorescence efficiency of cyanine dyes can increase by ~1,000-fold upon binding to proteins and nucleic acids (36). The stable binding together with the shift toward increased fluorescence could be highly beneficial, accounting for the "trapping" of the NIR signals in cancer cells for prolonged periods (>5 days) and allowing tumor detection in live animals with high signal/noise ratios. The stability of these cyanine dyes after formalin fixation raises the possibility of developing new and sensitive means of detecting cancer cells in whole blood and in harvested surgical specimens by injecting the cyanine dyes before sampling at the time of surgery. In practice, these could help physicians and pathologists follow up patients with possible circulating cancer cells in blood and assess surgical margins at the time of surgery. Our study suggests the differential dye uptake and retention by cancer and normal cells and tissues can be shown robustly by the use of a variety of detecting devices including Zeiss LSM 510 META, Kodak 4000MM, and Olympus OV100 systems. We adopted these different detecting methodologies based on their sensitivity and capability of allowing merging of image-sobtained via different detection modalities (e.g., X-ray and NIR imagings). The wide range of detecting devises used in our study supports the conclusion that IR-783 is

preferentially taken up and retained by cancer but not normal cells.

The mechanisms by which these cyanine dyes cross the cytoplasmic membranes of cancer cells but not normal cells were investigated. We concluded that the uptake was mediated by proteins of the OATP family, because the active uptake could be effectively blocked by BSP. OATPs are well recognized as channels for the transport of a diverse group of substrates, including bile acids, hormones, xenobiotics, and their metabolites (40–42). Results from this study are consistent with published reports, which indicate differences in the type and levels of OATPs between cancer and normal cells (43–46). Moreover, certain members of OATPs have recently been shown to be overexpressed in various human cancer tissues as well as in cancer cell lines (47–50), and the confirmation of OATPs as the key mediator of heptamethine cyanine dye uptake and retention in tumor cells warrants further investigation.

The ability of mouse tumors to accumulate these cyanine dyes is of great significance. This will facilitate the use of these dyes in immune-intact syngenic and transgenic mouse models to study the fundamentals of cancer biology, metastasis, and therapy. Because these dyes can be further explored as generalized ligands for all malignant cells, the synthesis of dye-antineoplastic drug conjugates, dye-radiolabeled drug conjugates, and dye-toxin conjugates could immensely facilitate the development of new therapeutics to treat cancer and precancerous conditions.

In summary, two heptamethine cyanine dyes were shown to selectively target cancer but not normal cells, irrespective of their species and organ of origin. This class of dual imaging and targeting cyanine dyes holds great promise for novel therapeutics for future cancer therapy and imaging. Future application of NIR fluorescent dyes in the clinic could lead to important progress in the management of cancer patients on an individual basis.

Disclosure of Potential Conflicts of Interest

Grant Support

References

1. Henary M, Mojzych M. Stability and reactivity of polymethine dyes in solution. Topic Heterocycl Chem, Springer Berlin/Heifelberg 2008; 14:221–38.
2. Licha K, Riefke B, Ebert B, Grotzinger C. Cyanine dyes as contrast agents in biomedical optical imaging. Acad Radiol 2002;9 Suppl 2: S320–2.
3. Rao J, Dragulescu-Andrasi A, Yao H. Fluorescence imaging *in vivo*: recent advances. Curr Opin Biotechnol 2007;18:17–25.
4. Frangioni JV. *In vivo* near-infrared fluorescence imaging. Curr Opin Chem Biol 2003;7:626–34.
5. Hawrysz DJ, Sevick-Muraca EM. Developments toward diagnostic breast cancer imaging using near-infrared optical measurements and fluorescent contrast agents. Neoplasia 2000;2:388–417.
6. Ntziachristos V, Bremer C, Weissleder R. Fluorescence imaging with near-infrared light: new technological advances that enable *in vivo* molecular imaging. Eur Radiol 2003;13:195–208.
7. Gao X, Cui Y, Levenson RM, Chung LW, Nie S. *In vivo* cancer targeting and imaging with semiconductor quantum dots. Nat Biotechnol 2004;22:969–76.
8. Hintersteiner M, Enz A, Frey P, et al. *In vivo* detection of amyloid-β deposits by near-infrared imaging using an oxazine-derivative probe. Nat Biotechnol 2005;23:577–83.
9. Wu X, Liu H, Liu J, et al. Immunofluorescent labeling of cancer marker Her2 and other cellular targets with semiconductor quantum dots. Nat Biotechnol 2003;21:41–6.
10. Humblet V, Lapidus R, Williams LR, et al. High-affinity near-infrared fluorescent small-molecule contrast agents for *in vivo* imaging of prostate-specific membrane antigen. Mol Imaging 2005;4:448–62.
11. Frangioni JV. New technologies for human cancer imaging. J Clin Oncol 2008;26:4012–21.
12. Kondepati VR, Heise HM, Backhaus J. Recent applications of near-infrared spectroscopy in cancer diagnosis and therapy. Anal Bioanal Chem 2008;390:125–39.
13. Pierce MC, Javier DJ, Richards-Kortum R. Optical contrast agents and imaging systems for detection and diagnosis of cancer. Int J Cancer 2008;123:1979–90.
14. Edwards PA. Heterogeneous expression of cell-surface antigens in normal epithelia and their tumours, revealed by monoclonal antibodies. Br J Cancer 1985;51:149–60.
15. Heppner GH, Miller FR. The cellular basis of tumor progression. Int Rev Cytol 1998;177:1–56.
16. Strekowski L, Lipowska M, Patonay G. Substitution reactions of a nucleofugal group in heptamethine cyanine dyes. Synthesis of an isothiocyanato derivative for labeling of proteins with a near-infrared chromophore. J Org Chem 1992;57.
17. Narayanan N, Patonay G. A new method for the synthesis of heptamethine cyanine dyes: synthesis of new near-infrared fluorescent labels. J Org Chem 1995;60.
18. Zhang Z, Achilefu S. Synthesis and evaluation of polyhydroxylated near-infrared carbocyanine molecular probes. Org Lett 2004;6.
19. Thalmann GN, Sikes RA, Wu TT, et al. LNCaP progression model of human prostate cancer: androgen-independence and osseous metastasis. Prostate 2000;44:91–103.
20. Zhau HY, Chang SM, Chen BQ, et al. Androgen-repressed phenotype in human prostate cancer. Proc Natl Acad Sci U S A 1996;93:15152–7.
21. Sung SY, Hsieh CL, Law A, et al. Coevolution of prostate cancer and bone stroma in three-dimensional coculture: implications for cancer growth and metastasis. Cancer Res 2008;68:9996–10003.
22. Nomura T, Huang WC, Seo S, Zhau HE, Mimata H, Chung LW. Targeting β2-microglobulin mediated signaling as a novel therapeutic approach for human renal cell carcinoma. J Urol 2007; 178:292–300.
23. Marcus AI, Peters U, Thomas SL, et al. Mitotic kinesin inhibitors induce mitotic arrest and cell death in Taxol-resistant and -sensitive cancer cells. J Biol Chem 2005;280:11569–77.
24. Moreno RD, Ramalho-Santos J, Chan EK, Wessel GM, Schatten G.

The Golgi apparatus segregates from the lysosomal/acrosomal vesicle during rhesus spermiogenesis: structural alterations. Dev Biol 2000;219:334–49.

25. Cui Y, Konig J, Leier I, Buchholz U, Keppler D. Hepatic uptake of bilirubin and its conjugates by the human organic anion transporter SLC21A6. J Biol Chem 2001;276:9626–30.

26. Wu TT, Sikes RA, Cui Q, et al. Establishing human prostate cancer cell xenografts in bone: induction of osteoblastic reaction by prostate-specific antigen-producing tumors in athymic and SCID/bg mice using LNCaP and lineage-derived metastatic sublines. Int J Cancer 1998;77:887–94.

27. Xu J, Wang R, Xie ZH, et al. Prostate cancer metastasis: role of the host microenvironment in promoting epithelial to mesenchymal transition and increased bone and adrenal gland metastasis. Prostate 2006;66:1664–73.

28. Saxena V, Sadoqi M, Shao J. Polymeric nanoparticulate delivery system for indocyanine green: biodistribution in healthy mice. Int J Pharm 2006;308:200–4.

29. Corti A, Ponzoni M. Tumor vascular targeting with tumor necrosis factor α and chemotherapeutic drugs. Ann N Y Acad Sci 2004; 1028:104–12.

30. Cuenod CA, Fournier L, Balvay D, Guinebretiere JM. Tumor angiogenesis: pathophysiology and implications for contrast-enhanced MRI and CT assessment. Abdom Imaging 2006;31:188–93.

31. Maio M, Altomonte M, Calabro L, Fonsatti E. Bioimmunotherapeutic targets on angiogenetic blood vessels in solid malignangies. Front Biosci 2001;6:D776–84.

32. Nanda A, St Croix B. Tumor endothelial markers: new targets for cancer therapy. Curr Opin Oncol 2004;16:44–9.

33. Gingrich JR, Barrios RJ, Morton RA, et al. Metastatic prostate cancer in a transgenic mouse. Cancer Res 1996;56:4096–102.

34. Ghaleb AM, McConnell BB, Nandan MO, Katz JP, Kaestner KH, Yang VW. Haploinsufficiency of Kruppel-like factor 4 promotes adenomatous polyposis coli dependent intestinal tumorigenesis. Cancer Res 2007;67:7147–54.

35. Johnson JL, West JK, Nelson AD, Reinhart GD. Resolving the fluorescence response of Escherichia coli carbamoyl phosphate synthetase: mapping intra- and intersubunit conformational changes. Biochemistry 2007;46:387–97.

36. Silva GL, Ediz V, Yaron D, Armitage BA. Experimental and computational investigation of unsymmetrical cyanine dyes: understanding torsionally responsive fluorogenic dyes. J Am Chem Soc 2007;129:5710–8.

37. Chen Y, Ohkubo K, Zhang M, et al. Photophysical, electrochemical characteristics and cross-linking of STAT-3 protein by an efficient bifunctional agent for fluorescence image-guided photodynamic therapy. Photochem Photobiol Sci 2007;6:1257–67.

38. Chandra P, Zhang P, Brouwer KL. Short-term regulation of multidrug resistance-associated protein 3 in rat and human hepatocytes. Am J Physiol Gastrointest Liver Physiol 2005;288:G1252–8.

39. Ito A, Yamaguchi K, Tomita H, et al. Distribution of rat organic anion transporting polypeptide-E (oatp-E) in the rat eye. Invest Ophthalmol Vis Sci 2003;44:4877–84.

40. Bertolino C, Caputol G, Barolo C, Viscardi G, Coluccial S. Novel Heptamethine cyanine dyes with large stokes' shift for biological applications in the near infrared. J Fluoresc 2006;16:221–5.

41. Delaey E, van Laar F, De Vos D, Kamuhabwa A, Jacobs P, de Witte P. A comparative study of the photosensitizing characteristics of some cyanine dyes. J Photochem Photobiol B 2000;55:27–36.

42. Kim RB. Organic anion-transporting polypeptide (OATP) transporter family and drug disposition. Eur J Clin Invest 2003;33 Suppl 2:1–5.

43. Al Sarakbi W, Mokbel R, Salhab M, Jiang WG, Reed MJ, Mokbel K. The role of STS and OATP-B mRNA expression in predicting the clinical outcome in human breast cancer. Anticancer Res 2006; 26:4985–90.

44. Ballestero MR, Monte MJ, Briz O, Jimenez F, Gonzalez-San Martin F, Marin JJ. Expression of transporters potentially involved in the targeting of cytostatic bile acid derivatives to colon cancer and polyps. Biochem Pharmacol 2006;72:729–38.

45. Marzolini C, Tirona RG, Kim RB. Pharmacogenomics of the OATP and OAT families. Pharmacogenomics 2004;5:273–82.

46. Mikkaichi T, Suzuki T, Tanemoto M, Ito S, Abe T. The organic anion transporter (OATP) family. Drug Metab Pharmacokinet 2004;19: 171–9.

47. Abe T, Unno M, Onogawa T, et al. LST-2, a human liver-specific organic anion transporter, determines methotrexate sensitivity in gastrointestinal cancers. Gastroenterology 2001;120:1689–99.

48. Monks NR, Liu S, Xu Y, Yu H, Bendelow AS, Moscow JA. Potent cytotoxicity of the phosphatase inhibitor microcystin LR and microcystin analogues in OATP1B1- and OATP1B3-expressing HeLa cells. Mol Cancer Ther 2007;6:587–98.

49. Lee W, Belkhiri A, Lockhart AC, et al. Overexpression of OATP1B3 confers apoptotic resistance in colon cancer. Cancer Res 2008;68: 10315–23.

50. Muto M, Onogawa T, Suzuki T, et al. Human liver-specific organic anion transporter-2 is a potent prognostic factor for human breast carcinoma. Cancer Sci 2007;98:1570–6.